Award Number: G16AP00094

Developing a Seismic Velocity Model of the Central Valley, Northern California

Justin Lindeman, Donna Eberhart-Phillips, Louise H. Kellogg, and Lorraine J. Hwang

March 1, 2016 - February 28, 2017

University of California, Davis
1 Shields Ave
Earth and Planetary Sciences
Davis, CA 95616
Fax: 530.752.0951

530.752.0350 jrlindeman@ucdavis.edu
530.752.0350 eberhartphillips@ucdavis.edu
530.752.3690 lhkellogg@ucdavis.edu
530.752.3656 ljhwang@ucdavis.edu

Abstract

In this report, we present five seismic velocity models for Northern California with emphasis on the Sacramento-San Joaquin Delta region (SSJD). A regional 3-D tomographic model (SSJD2016) of P-wave velocity (V_p) and V_p/V_s was calculated from a joint inversion of travel-time and group velocity observations using the Simul velocity inversion code. Calculated gravity measurements compared to gravity observations helped improve areas that lacked seismic data. SSJD2016 extends from the Great Valley's western margin to the Sierra with a horizontal node spacing of 10 km and vertical node spacing of $3-8$ km to 36 km depth. Compressional and shear-wave velocity versus depth relations were used to integrate Tertiary submarine canyons within the Cenozoic Great Valley sequence. The four shallow velocity models - SSJDOPHW95, SSJDGRANW95, SSJDFRANW95, and SSJDFRANG16, extend from the surface to 3.2 km. SSJDOPHW95, SSJDGRANW95, and SSJDFRANW95 utilize the basement interpretations from *Wentworth et al.* [1995] and assume ophiolitic, granitic, and Franciscan rock, respectively, beneath the Great Valley sequence. SSJDFRANG16 applies Graymer (*written communication*, 2016) and assumes only Franciscan rock to calculate velocities beneath the Great Valley sequence.

1 Introduction

California's San Andreas Fault System (SAFS) contains some of the most active faults in the United States. Many of its segments which are prone to large and destructive earthquakes traverse heavily populated regions. The northern SAFS dissects the San Francisco Bay Area (SFBA) and extends ∼75 km eastward across the California Coast Ranges into the Great Valley and the Sacramento-San Joaquin Delta (SSJD). Recent activity (i.e. 2000 M_w 5.0 Yountville and the 2014 M_w 6.0 Napa Valley earthquakes) on the West Napa fault raises concerns for a large (M>6) magnitude earthquake near and/or in the SSJD (*Baltay and Boatwright* [2015]; *Barnhart et al.* [2015]; *Boatwright et al.* [2015]; *Brocher et al.* [2015];

Dreger et al. [2015]; *Langenheim et al.* [2006]; *DRMS* [2006]; *Wesling and Hanson* [2008]). Faults of the San Joaquin fault zone and the Sacramento Basin (e.g., Dunnigan, Midland, Sweitzer, Willow Hills) and the larger faults bordering the SSJD (e.g., Concord-Green Valley, Hayward-Rodgers Creek, Calaveras) (*MacKevett* [1992]; *Pepper and Johnson* [1992]; *Wong* [1992]) are poorly studied and are capable of generating a M_w 6.7 earthquake or greater (*Field et al.* [2014]). The 1892 M_L 6.5 Vacaville-Winters earthquake occurred on an unidentified fault in the region (*Bennett* [1987]). The damage described is comparable to the 1983 Coalinga earthquake of similar magnitude (M_w 6.2) that caused $31 million in damage in that sparsely populated region (*Bennett* [1987]). Some have speculated that the Midland fault is the causative fault, however, little conclusive information exists.

At the confluence of the Sacramento and San Joaquin Rivers, the construction of nearly 1800 km of levees over the last century have transformed the SSJD from a tidal marsh into an agricultural-rich region and freshwater source for much of California. In doing so, human activity has added levee failure to the list of seismic risks in the region. Additionally, subsidence at a rate of $2-5$ cm/yr (*Rojstaczer et al.* [1991]; *Sharma et al.* [2016]) has resulted in elevating the heights of levees, increasing stresses along the levee banks and hence, their potential for failure. An earthquake would subject the already fragile levees to dynamic loading possibly leading to failure and flooding (*Torres et al.* [2000]; *DRMS* [2006]).

The SSJD generates $35 billion annually (*DRMS* [2006]). The Delta Risk Management Strategy (*DRMS* [2006]) estimated that levee failure induced flooding could cost between $6.7 and $56.3 billion and damage could extend into the Sacramento and Stockton areas. A salt water incursion due to levee failure would have devastating consequences for the State's freshwater supply impacting agriculture, the delta islands, sloughs, and man-made channels. The SSJD is also home to major water infrastructure - the Delta-Mendota Canal and the California Aqueduct; transportation infrastructure - two interstates and three state highways; and power infrastructure such as generation, storage, and electrical transmission lines and facilities.

Strong ground motion in the SSJD has the potential of wide-spread damage to buildings and to infrastructure. Both soil saturation and weak soils are recognize as important site characteristics resulting in soil failure and damage to a built environment. Soft sediments compound this problem by amplifying seismic waves. The upper $\sim$100 m of the SSJD is composed of Holocene peats and unconsolidated sediments eroded from the Coast Ranges. The geometry of these deposits can further distort ground motions at soft rock sites and is important for wave-focusing effects. In addition, reverberation of seismic waves at basin edges can lead to interference patterns that could enhance the ground motion at longer periods.

The Great Valley's flat surface hides a complex subsurface that has been explored for oil, gas, and water. Its depth sharply increases westward under the SSJD extending possibly to depths of 10 km or greater (*Wentworth et al.* [1995]; *Moores et al.* [2002]; *Jachens et al.* [2006]; *Thurber et al.* [2007]). This deep structure impacts the lower frequency seismic waves potentially causing more widespread effects. Steep edges of the basin could easily generate complex surface waves. Seismic waves traveling at high velocities through crystalline rock refract and slow dramatically when encountering the soft rocks of the basin. This increases the amplitude of the earthquake waves and traps energy in the basin extending the

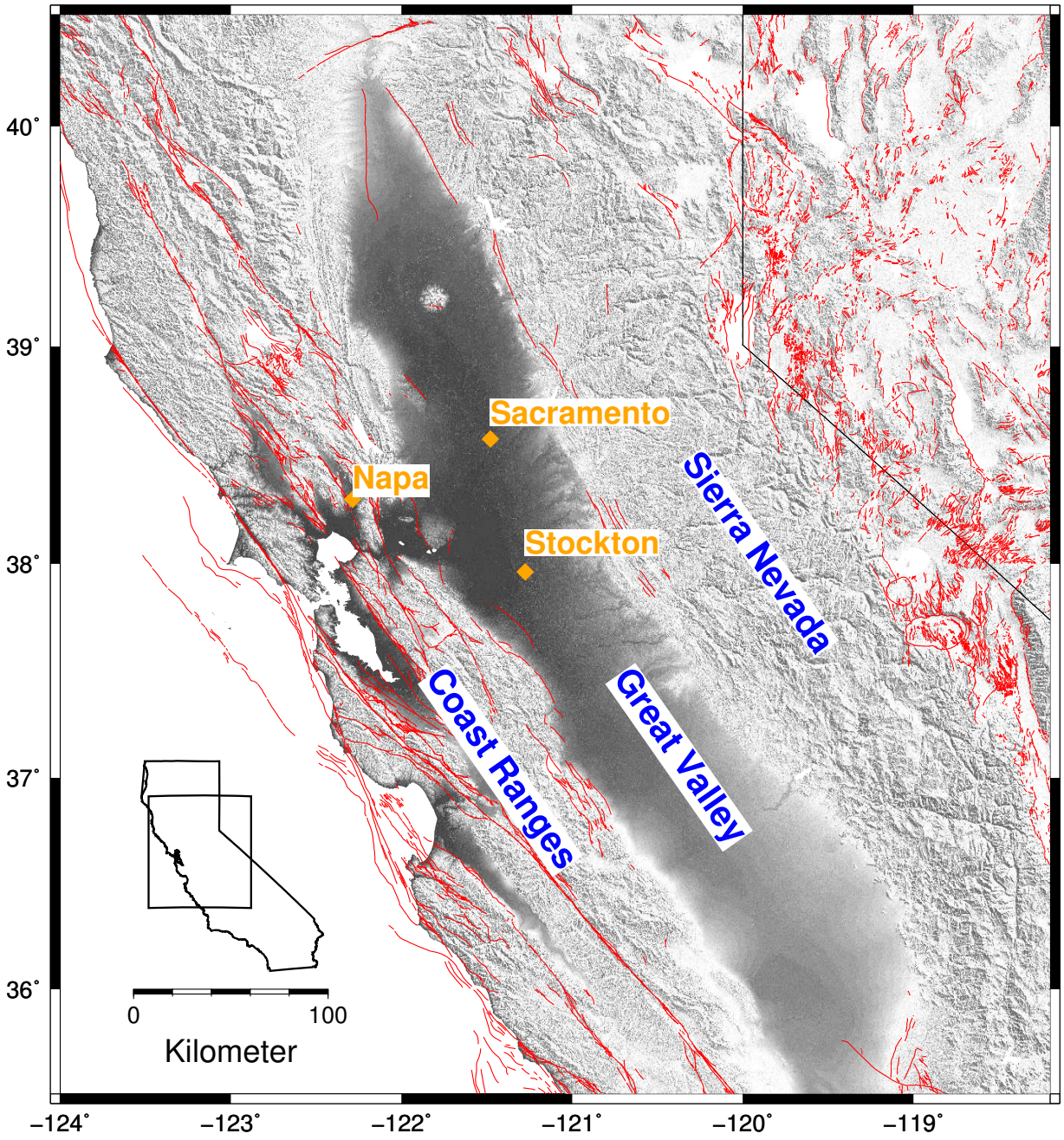

Figure 1: Regional map of the study area in northern California showing active Quaternary faults (red), selected regions (blue), and selected cities (orange).

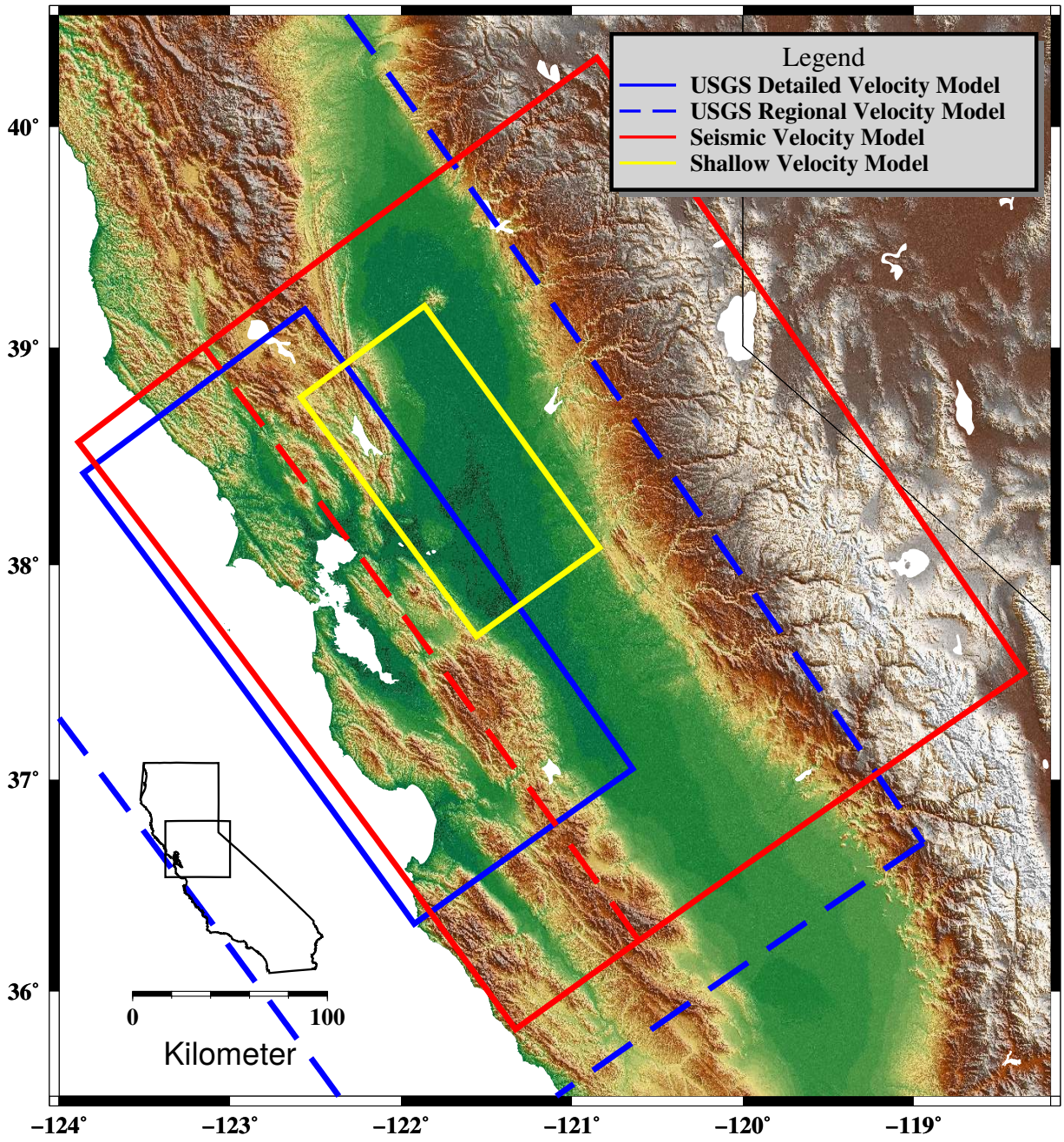

Figure 2: Map showing the regions of the northern California velocity models in this study. Blue box shows the area of the USGS 08.03.1 detailed velocity model, dashed blue box the USGS 08.03.1 regional velocity model, and yellow box the region of the shallow velocity model study. The red box shows the study area of SSJD2016. Velocities were held fixed in the region west of the red dashed line.

duration of shaking. Hence, realistic models of the subsurface are needed for understanding the variations in strong ground motion in order to estimate damage patterns from future earthquakes and simulate phenomena affecting human safety.

This study improves the existing regional seismic velocity models by: (1) updating existing seismic tomography models by first using recent earthquake data as well as ambient noise and group velocity data, and then integrating land-based gravity measurements; and (2) developing shallow crustal velocity models by employing velocity-versus-depth relations with two basement interpretations and introducing three major regional buried submarine canyons. These models provide areas of higher resolution volume characteristics (e.g. seismic velocity and attenuation), geometries of structures, and boundary conditions useful for seismic-wave propagation modeling.

1.1 Previous Work

The most recent iterations of the USGS 3-D velocity models, version 08.3.0 (detailed and regional), developed for recent California ground motion studies (*Aagaard et al.* [2010a, b, 2013]) were constructed using a broad range of geological and geophysical data including:

- geologic and geophysical mapping (*Jachens et al.* [2006]);
- lithology to: density, seismic compressional- and shear-wave speeds, and attenuation relationships (*Brocher* [2005a, b, c, 2008]);
- waveform modeling (*Rodgers et al.* [2008]), and
- seismic tomography (*Thurber et al.* [2007]).

These studies are described below.

Jachens et al. [2006] produced a three-dimensional geologic map of northern California that consists of specific geologic units separated by discrete boundaries. Their structural model was derived from geologic mapping, gravity and magnetic surveying, double-difference relocated seismicity, seismic soundings, seismic tomography, and well logs (*Jachens et al.* [2006]). Depth to crystalline basement is taken from *Wentworth et al.* [1995] (Fig. 6) where the basement is defined in the eastern Great Valley by well logs (> 500), some of which reached basement, and in the western valley, by a much smaller number of seismic refraction and reflection profiles. This 3-D block model provided structures where empirical relations (seismic-wave velocities, intrinsic attenuations, and densities) based on geology and depth could be assigned.

Brocher [2005a, b, c] calculated velocity-depth relations for different lithologic units by fitting regression curves to available observations of borehole, seismic refraction and tomography, and density measurements for each main northern California rock type: Holocene sedimentary deposits; Plio-Quaternary sedimentary deposits; older Cenozoic sedimentary rocks; Mesozoic Great Valley sequence sedimentary rocks; metagreywacke (Franciscan Complex); and granitic rocks (*Brocher* [2005a, b, c, 2008]). Quaternary-Tertiary regressions were derived from sonic logs for several basins, including the Great Valley and the western SSJD *Brocher* [2005c]. The Great Valley sequence (GRV) regressions are derived from a larger

sonic log collection and seismic refraction studies that suggest older GRV rocks (Mesozoic and Cenozoic) have slightly higher velocities than the Quaternary-Tertiary dataset. Later, *Brocher* [2008] calculated attenuation, Q, as a function of V_p and V_s. Q_s and Q_p were derived from forward modeling of strong ground motions during the 1989 Loma Prieta and 1906 San Francisco earthquakes by *Brocher* [2008]. These relations were applied to the 3D-geologic map of *Jachens et al.* [2006] to produce the USGS 3-D Seismic Velocity Model 05.1.0.

Rodgers et al. [2008] tested the validity of the USGS 05.1.0 model by comparing three-component broadband waveforms of moderate earthquakes (M_w 4 to 5) with synthetic seismograms calculated from USGS 05.1.0. Results showed predicted waves speeds were $\sim$5% faster than observed.

Coevally, *Thurber et al.* [2007] used data from the Northern California Earthquake Data Center (NCEDC) that included phase arrival times from $>$ 5500 chemical blasts and arrival times from $>$ 6000 earthquakes to develop a regional 3-D seismic velocity model for the San Francisco Bay Area (SFBA2007) using double-difference seismic tomography.

The USGS 3-D velocity model 08.3.0 combined the findings and models of *Jachens et al.* [2006], *Brocher* [2008], *Rodgers et al.* [2008], and *Thurber et al.* [2007] to ground-motion modeling of earthquakes along the Hayward fault (*Aagaard et al.* [2010a, b]). *Aagaard et al.* [2010a, b] improved the *Brocher* [2008] velocity-vs-depth relations to minimize the inconsistencies between the synthetic waveforms calculated with the 05.1.0 model and the observed earthquake waveforms. In their study, calculated wave speeds were compared for each geologic unit in the 05.1.0 model with wave speeds in the SFBA2007 model. The relations were improved to fit the gradients in the SFBA2007 model below several kilometers and the *Brocher* [2008] equations at depths closer to the surface. A detailed explanation can be found in *Aagaard et al.* [2010b].

1.2 Data Used from Previous Studies

This study used three previously-collected datasets to solve for the velocity structure in the SSJD. We integrated the *Thurber et al.* [2009] velocity model with the group velocity dataset from *Fletcher et al.* [2016] in a joint inversion. To construct a geologically-based velocity model, we used the *Downey and Clinkenbeard* [2010] structural dataset under the SSJD and applied velocity-vs-depth relations.

Thurber et al. [2009] expanded the SFBA2007 model creating a regional 3-D P-wave velocity model of northern California (NC2009). *Thurber et al.* [2009] used over 5600 earthquakes of magnitude 2.0 and above observed at 688 stations obtained from the Northern California Earthquake Data Center (NCEDC). Their model has horizontal node-spacing of $10 - 20$ km and $3 - 8$ km vertically and used finite-difference methods to compute travel times for over 5600 earthquakes and controlled-source experiments. The NC2009 velocity model revealed important regional features including a previously modeled high velocity ophiolite body underlying the Great Valley (*Godfrey et al.* [1997]; *Godfrey and Klemperer* [1998]; *Moores et al.* [2002]) and a never-before imaged deeply-penetrating fault beneath the SSJD identified as the Pittsburg/Kirby Hills Fault. NC2009 was used as our starting velocity model, however, NC2009 has poor resolution at shallow depths in the SSJD region. *Lin et al.* [2010] calculated a 3-D statewide velocity model that combined the NC2009 model with the *Lin et al.* [2007] southern California model. The *Lin et al.* [2010] model resulted in

a better velocity structure at the boundaries of these previous studies. Where NC2009 had no representative velocities in the SSJD, *Lin et al.* [2010] was used as our initial model.

To this dataset we added the group velocities of *Fletcher et al.* [2016]. *Fletcher et al.* [2016] studied ambient noise from their temporary array in the SSJD (*Fletcher and Boatwright* [2013]) to build a Rayleigh-wave group velocity model. In large parts of the SSJD, this data has better resolution than the seismic tomography. This group velocity data was added to the travel time data and jointly inverted as described in the next sections.

To refine the shallow velocity structure, we used *Downey and Clinkenbeard* [2010]. *Downey and Clinkenbeard* [2010] investigated the CO_2 sequestration potential under the SSJD and identified gross sandstone thickness to depths of ∼3 km. The depth-to-sandstone maps and gross sandstone isopachs were used to develop a model of the shallow structure by providing structural constraints for three submarine canyons beneath the SSJD. These features are younger than the surrounding rocks and were assigned different *Aagaard et al.* [2010b] velocity-vs-depth relations then the surrounding Great Valley Sequence based on age and geology.

2 Methods

2.1 Joint Inversion for Regional-Scale Tomography

2.1.1 Joint Inversion of Group Velocity and Earthquake Travel-time Data

The Simul velocity inversion codes use travel times of local earthquakes and controlled sources in a simultaneous inversion for hypocenters, 3-D P-velocity, V_p, and V_p/V_s (*Thurber and Eberhart-Phillips* [1999]; *Eberhart-Phillips and Reyners* [2012]), solving for velocity on a 3-D grid of nodes with velocity linearly interpolated between nodes, and allowing flexible gridding through linking and fixing of nodes. The velocity is obtained by damped least squares, using LU decomposition to obtain a solution that has few artifacts and stays close to the initial model where there is little resolution. Earthquake differential times and receiver differential times may be included to increase resolution near earthquake hypocenters and at shallow depths near stations. Each travel-time residual is related to perturbations to the velocity at grid points along the raypath. In areas where there are many crossing raypaths the velocity will be well resolved spatially; where there are few raypaths velocity features will be imaged broadly. In particular, there may be vertical smearing at shallow depths towards the station such that shallow velocity features may be weakly imaged without sharp gradients unless there are numerous earthquakes and stations or active source constraints.

The Simul code has since been updated for joint inversion of travel-time and group velocity observations (*Eberhart-Phillips and Fry* [2016]). Group velocity (GV) observations are included using each point from the GV 2-D models, for all periods. The GV 2-D models are a standard method of combining the uneven spatial sampling of interstation dispersion curves, and are thus appropriate as input observations for 3-D velocity inversion. For each point, an observation quality can be assigned based on the number of good dispersion paths that contribute to that volume. Surface waves sample a crustal volume along the surface path which may be 15 to 60 km wide, for periods 6 to 20 sec. Thus they have large horizontal averaging compared to vertical averaging for travel-time. The GV is related to both V_p and V_s from the surface throughout crust, with longer periods sampling deeper. The shallow crust

is sampled by all the periods and will have the most information. The complicated sampling described by sensitivity kernels (partial derivatives) can be computed using Herrmann's computer programs in seismology (CPS; *Herrmann* [2013]), as shown for 10 sec period in Figure 3. The 10 sec GV is strongest from 5 to 10 km depth for V_s, and 0 to 5 km depth for V_p. The width sampled is related to wavelength, so longer wavelengths sample larger width as well as greater depth. We use CPS srfker96 routines for computing the model GV and the partial derivatives that are used to relate the GV observations to the 3-D velocity model.

The GV residuals need to be related to the 3-D grid of V_p and V_p/V_s nodes, which are finer spaced than the GV observation points, and the fine spacing needs to be retained for the detailed travel-time velocity model. We take a box around each GV surface wave observation point. To compute the GV residual for point A, we take a 1-D average of the 3-D model in the box and use that in srfker96. Then the 1-D kernels are related to all the 3-D velocity nodes within the box, in an analogous manner to the travel-time residual being related to 3-D nodes along its raypath; with the V_s kernels related to partial derivatives of the V_p and V_p/V_s model parameters. Thus, the GV residuals can be fit through perturbations to any points in the box volume while simultaneously retaining sharp features of the travel-time velocity model which typically may have 5 km grid spacing. Given the larger volume sampled by the GV, the 1-D velocity model specifically at point A need not fit the GV observation and the 3-D model need not be as smooth as the GV 2-D observations. The box size is related to an input parameter and the period of the GV observation. The box depth for a given period GV observation extends to the depth where the V_s kernel is less than 4% of the maximum V_s kernel. Then the 3-D velocity model can be updated by simultaneous inversion of the GV observations and travel-time observations using iterative damped least squares. At each iteration, the residuals and partial derivatives are recalculated.

2.1.2 Gravity Inversion for 3D Seismic Inversion

Gravity observations also sample the 3-D volume and can aid in areas with little seismic data. The calculated gravity from the 3-D model is obtained using the density-velocity relationship of *Brocher* [2005b]. Both the observed and calculated gravity are upward continued 2 km to de-emphasize near-surface density variations that have finer scale than the velocity grid. The isostatic residual gravity is used because it is related to crustal heterogeneity. Each gravity observation is related to a large volume with the width of influence increasing with depth. The gravity residuals are used in an inversion for 3-D velocity perturbations (*Eberhart-Phillips and Michael* [1993]; *Eberhart-Phillips and Bannister* [2002]). This is not a joint inversion method and the seismic velocity can be influenced by many factors other than density, such as fluid pressure and crack density.

2.1.3 Data

For this study, we used travel-time data from 281 earthquakes with magnitudes between $2.0 - 5.2$ during 2005-2016 recorded by the NCSN (*NCDEC* [2014]) which provided 49,215 observations. Additionally, we incorporated travel-time data from refraction profiles that were used by *Thurber et al.* [2009] which provided an additional 19,189 observations. Surface wave GV observations were obtained from *Fletcher et al.* [2016]. They used ambient noise interstation dispersion curves of GV to obtain 2-D models of GV at periods of 4.5 to 10.5 s. These will be best constrained where the location is sampled by multiple interstation paths, and hence, we assign observation quality based on the number of paths near each GV

point for 3273 GV observations. Gravity data was provided by Victoria Langenheim, USGS (*written communication*, 2016), and consisted of gridded observations of isostatic residuals with 2 km spacing and upward continued 2 km.

2.1.4 Inversion Procedure

We carried out a series of three velocity inversions, as described above, using a modified NC2009 as our starting model. NC2009 modeled the regional structure along a 10x20 km grid. Along paths where there was no data, the model could not be updated and stayed as the initial northern California 1-D model. Thus, many shallow parts of the SSJD lack representative velocities. Hence, for our initial model we modified NC2009 using *Lin et al.* [2010] model for depths -1 to 4 km in the SSJD.

While the group velocity data samples the whole crust, it provides the most improvement to the NC2009 model in the shallow crust. In the first inversion, the GV and travel-time seismic data were used to update the 3-D velocity model at depths of -1 to 4 km, with the deeper model fixed. In a second seismic inversion, the solution included depths of -1 to 36 km, obtaining a seismic model that fits both seismic data sets. This decreased the data variance of the P travel-time by 24.1%, the S-P travel-time by 14.2%, and the GV by 69.5% from the initial model. Finally, the seismic model was used as the initial model for an inversion of the isostatic residual gravity to obtain a seismic velocity model that is also consistent with gravity. The final model, SSJD2016, provided a 98.8% decrease in data variance of the gravity data while somewhat weakening the fit to seismic data. Overall the seismic-gravity 3-D inversions decreased the data variance of the P travel-time by 16.6%, the S-P travel-time by 13.1%, and the GV by 64.0%.

The results for depths of 1 km and 4 km are shown in Figure 4. The area outside the SSJD is included but was fixed to NC2009. An example of the GV at the 8.5 s period observation points calculated from the final 3-D velocity model is shown in Figure 5. The largest GV residuals tend to be in areas where there is competition with refraction data, for example, in the southwest.

2.2 Shallow Velocity Models

2.2.1 Data

The area of the shallow velocity model is defined by the study area of *Downey and Clinkenbeard* [2010]. Their study identified thick sedimentary sections suitable for carbon sequestration in California. Amongst these, basins in the Sacramento and San Joaquin Valleys were found to have some of the thickness formation sequences mainly composed of the Cretaceous deposits of the Mokelumne River (MRF), Starkey (SF), and Winters (WF) formations. Regionally, these formations are incised and filled with the Tertiary sediments of the Markley, Martinez, and Meganos submarine canyons. Using information from over 6200 gas well logs, *Downey and Clinkenbeard* [2010] identified thick sandstone sequences of up to 460 m within the MRF, SF, and WF and developed isopachs of gross sandstone and sealing formation thickness along with their depths. Also identified were regions in which submarine canyons incised each formation. The horizontal boundaries of these submarine canyons along with the gross sandstone isopachs are used to estimate the thickness of the canyons through each formation. Since all canyons cut the MRF, the top of the canyons are taken to be the depth to the top of the MRF sandstones. The thickness of each canyon are

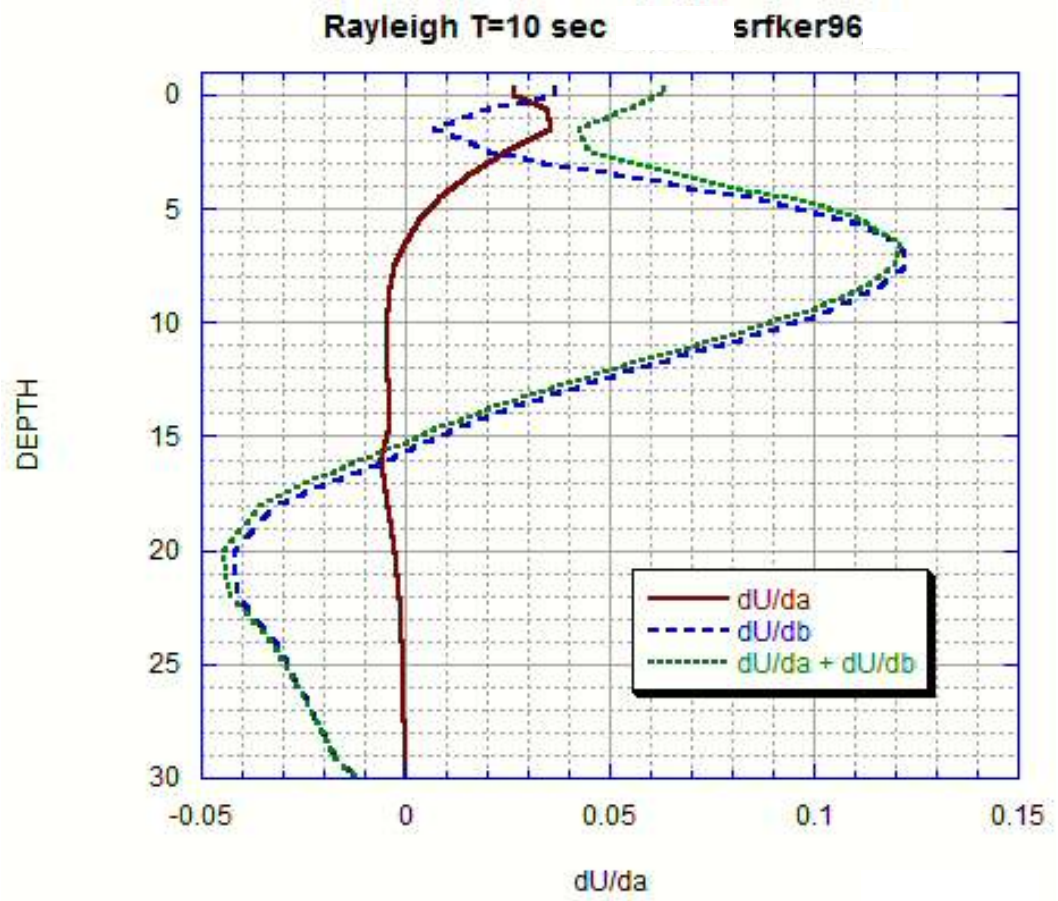

Figure 3: Sensitivity kernels at T=10 sec using *Herrmann* [2013] srfker96, V_p (red), V_s (blue), and V_p/V_s (green).

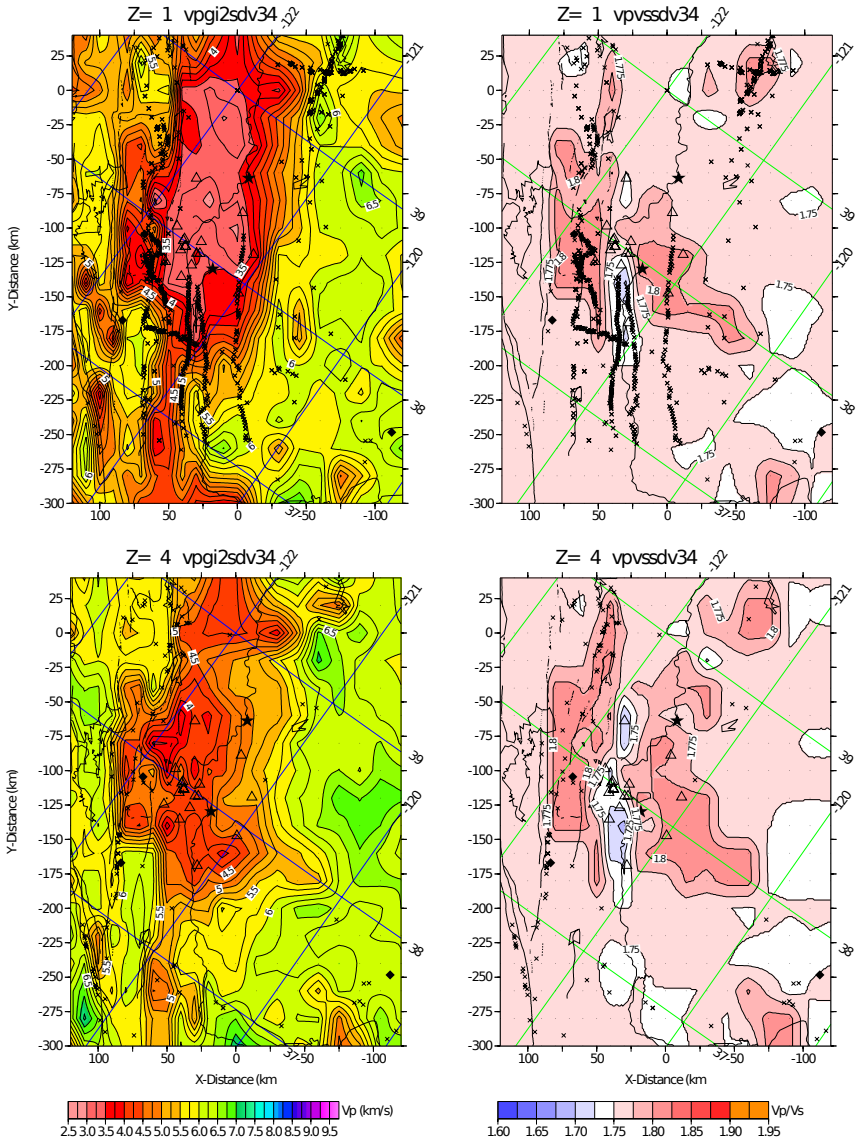

Figure 4: Depth slices of SSJD2016 showing V_p (left) and V_p/V_s (right) at depths = 1 and 4 km, with sources (earthquakes and refraction shots) used in the inversion shown by x's. The area outside the Delta is included but was fixed to NC2009; the inversion area is bounded by x= 80 to -120, y= -300 to 40, and z= -1 to 36. Coastline, active faults, and Sacramento and San Joaquin Rivers are shown. Stars are Sacramento and Stockton, solid diamonds are Mt. Diablo, Mt. Hamilton, and Mt. Whitney.

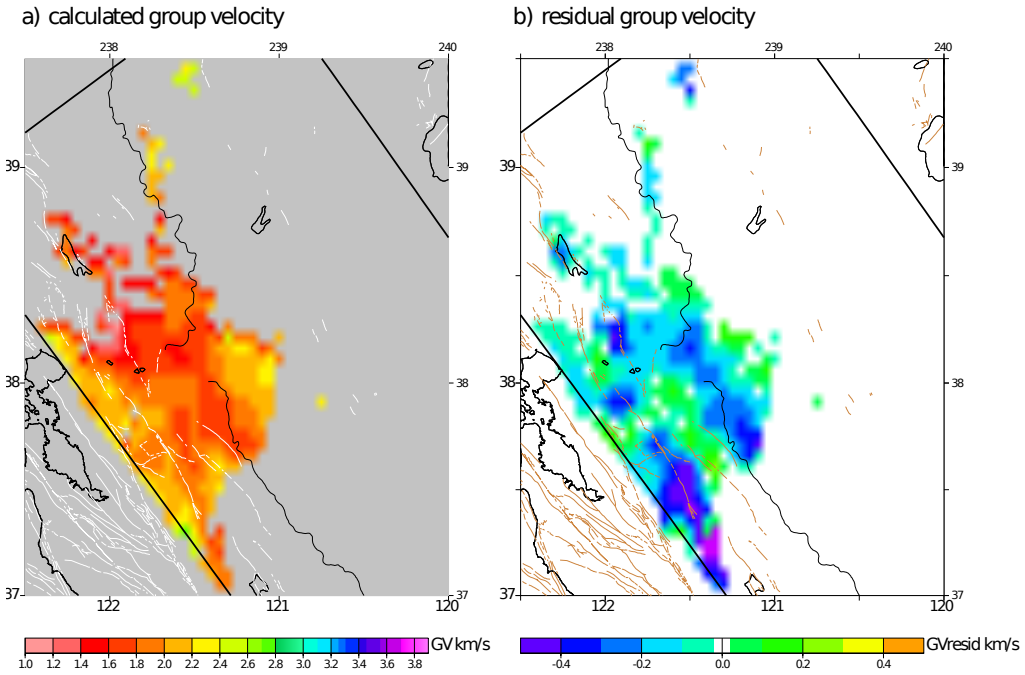

Figure 5: Plot of the a) calculated group velocity and b) the residual group velocity at the group velocity observation points which are the locations where the 2-D group velocity (*Fletcher et al.* [2016]) included multiple dispersion measurements.

assumed to extend to the bottom of the last formation in which that canyon appears. The Markley submarine canyon is present from the top of the MRF to the bottom of the SF. The Martinez and Meganos submarine canyons are only present in the MRF, but appear lower than the Markley in the west because of the Midland fault offset.

2.2.2 Calculating Velocity with Geology

The shallow velocity models presented in this study (SSJDOPHW95, SSJDGRANW95, SSJDFRANW95, and SSJDFRANG16) apply the compressional (V_p) and shear-wave (V_s) seismic velocity versus depth relations and intrinsic attenuation for common rock types in northern California originally presented by *Brocher* [2008] and later modified by *Aagaard et al.* [2010a, b]. The equations in Table 1 are a subset of the *Aagaard et al.* [2010b] equations currently used in the USGS 08.3.0 Seismic Velocity Model and are used to calculate V_p, V_s, Q_s, and Q_p in the shallow velocity models presented here. For equations that are at the surface, the velocity is assumed. For example, we assume all rocks outside the submarine canyons are Great Valley sequence (GRV). Equation 7 solves for GRV V_p in the range of 2.5 km/s (at surface; $z = 0$) to 4.36 km/s (at 3.2 km; $z = 3.2$). Equations 8 and 9 solve for GRV V_s in the range of 0.6 km/s (at surface; $z = 0$) to 2.41 km/s (at 3.2 km; $z = 3.2$). Equation 21 solves for GRV Q_s in the range of 39.17 (at surface; $z = 0$) to 203.17 (at 3.2 km; $z = 3.2$). Equation 22 solves for GRV Q_p in the range of 78.34 (at surface; $z = 0$) to 406.34 (at 3.2 km; $z = 3.2$). Inside the submarine canyons, equations $1 - 6$ calculate V_p and V_s with a range of $0.7 - 4.1$ and $0.08 - 0.68$ km/s, respectively.

It is unclear at what depth the transition from GRV to crystalline rock occurs or even

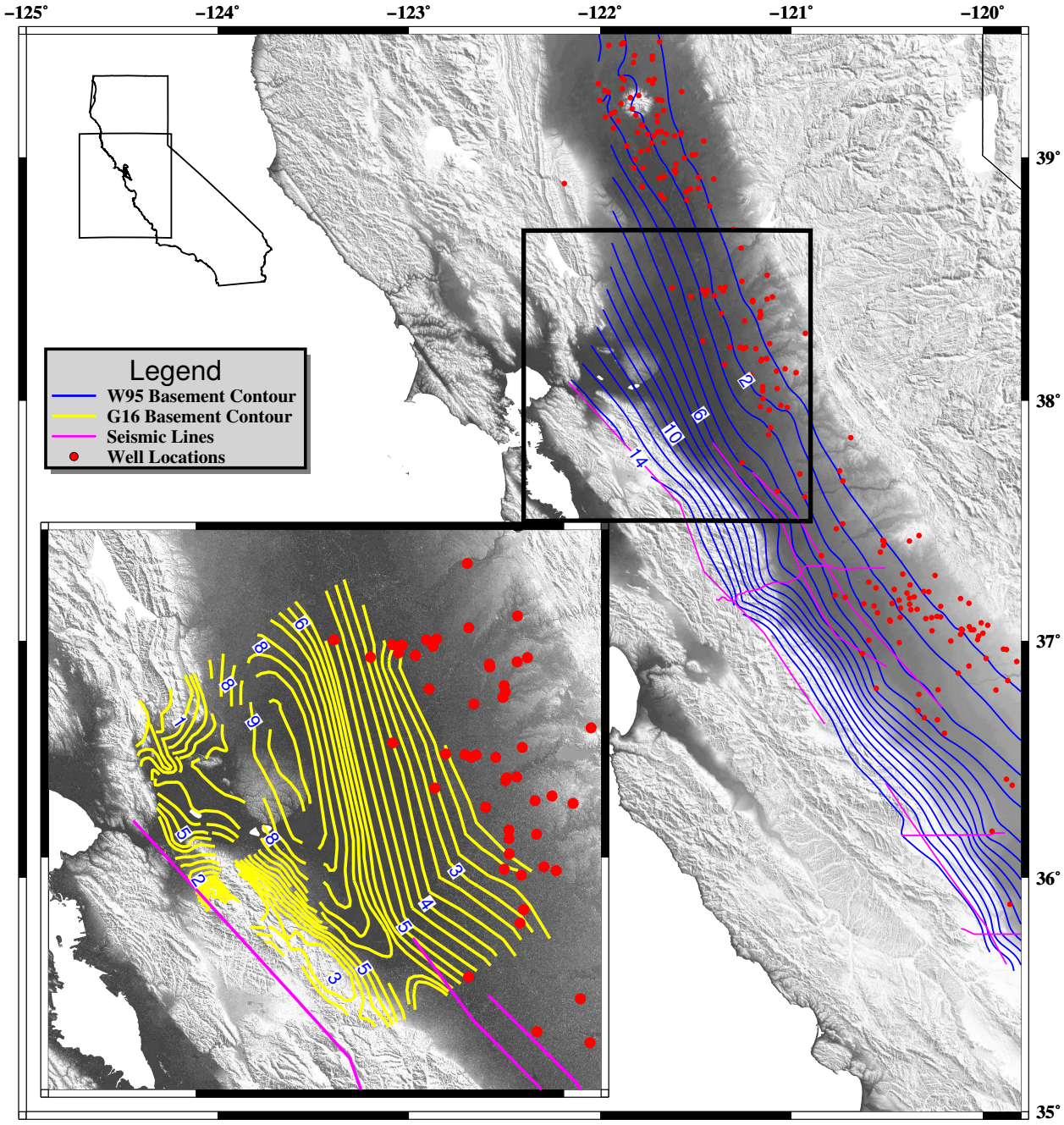

Figure 6: Basement surface contours, well locations, and seismic lines from *Wentworth et al.* [1995]. Basement is better constrained to the east where most of the wells are located. Inset adds the basement surface contours from Graymer (*written communication*, 2016).

what rock type underlies the GRV. To address this ambiguity, two different datasets are used to define basement under the SSJD. The first dataset from *Wentworth et al.* [1995] maps the crystalline basement from outcrops to the east in the Sierra Nevadan foothills and then proceeding west along a steeply dipping interface. Their model does not reach to the western region of our shallow velocity models; the lower boundary of our shallow velocity models are well above the interpreted basement surface in the west. The second dataset from Graymer (*written communication*, 2016) used well logs, seismic refraction lines, and downward projection of surficial gravity measurements to interpret basement depth beneath the SSJD to provide a detailed basement map in the western SSJD. In contrast to the Wentworth dataset, Graymer maps western basement shallower then 3.2 km under the western SSJD. There are subtle disagreements in the two basement maps (Fig. 6) and overlap between the two basements maps is minimal. In addition, the Graymer dataset conflicts with the carbon sequestration isopachs (see Discussion). For this last reason, we did not attempt to combine the two basement maps.

As a result of the differences in the basement interpretations, four models have been pro-

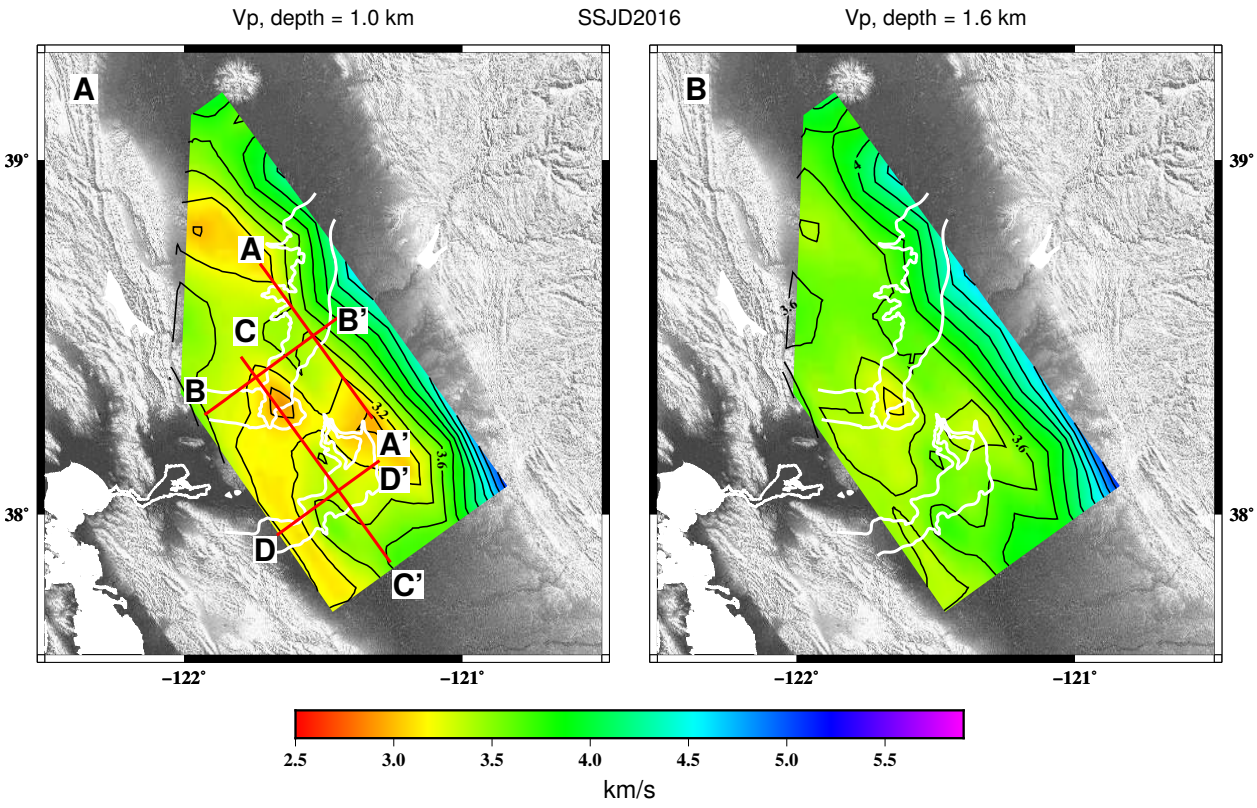

Figure 7: Map-view slices of SSJD2016 at 1.0 and 1.6 km depths for the region of the shallow velocity study. Contour interval is 0.2 km/s. White lines bound the three submarine canyons as projected in the MRF depth-to-sandstone map (*Downey and Clinkenbeard* [2010]). The location of cross-section slices in Fig. 8 are shown. The SSJD2016 locations correspond to: (1) A-A', x = 0 km; (2) B-B', y = -68 km; (3) C-C, x = -22 km; and (4) D-D', y = -122 km.

duced: three models use the *Wentworth et al.* [1995] basement interpretations calculated with three different basement geologies ophiolitic (SSJDOPHW95), granitic (SSJDGRANW95), and Franciscan basement (SSJDFRANW95); and one model with the Graymer basement interpretations calculated assuming Franciscan basement (SSJDFRANG16). The basement velocities are calculated in one of three ways. First, we assume that ophiolitic material (as defined by *Aagaard et al.* [2010b]) underlies the GRV and utilize the Great Valley and mafic regressions (Table 1, eq. 19 and 20). Second, we assume granitic rock underlies the GRV and apply the granitic regressions (Table 1, eq. 14-18). Third, we assume Franciscan material beneath the GRV (Table 1, eq. 10-13).

Above the basement interface, the addition of submarine canyons creates slow anomalies which are 0.2 to 0.6 km/s slower than the surrounding GRV. Beneath the basement interface the V_p structure changes. SSJDOPHW95 is consistently 5.9 km/s from the basement interface to the lower bounds of the model. SSJDGRANW95 ranges from 4.65 to 5.66 km/s beneath the basement. SSJDFRANW95 basement velocities range from 4.47 to 5.37 km/s.

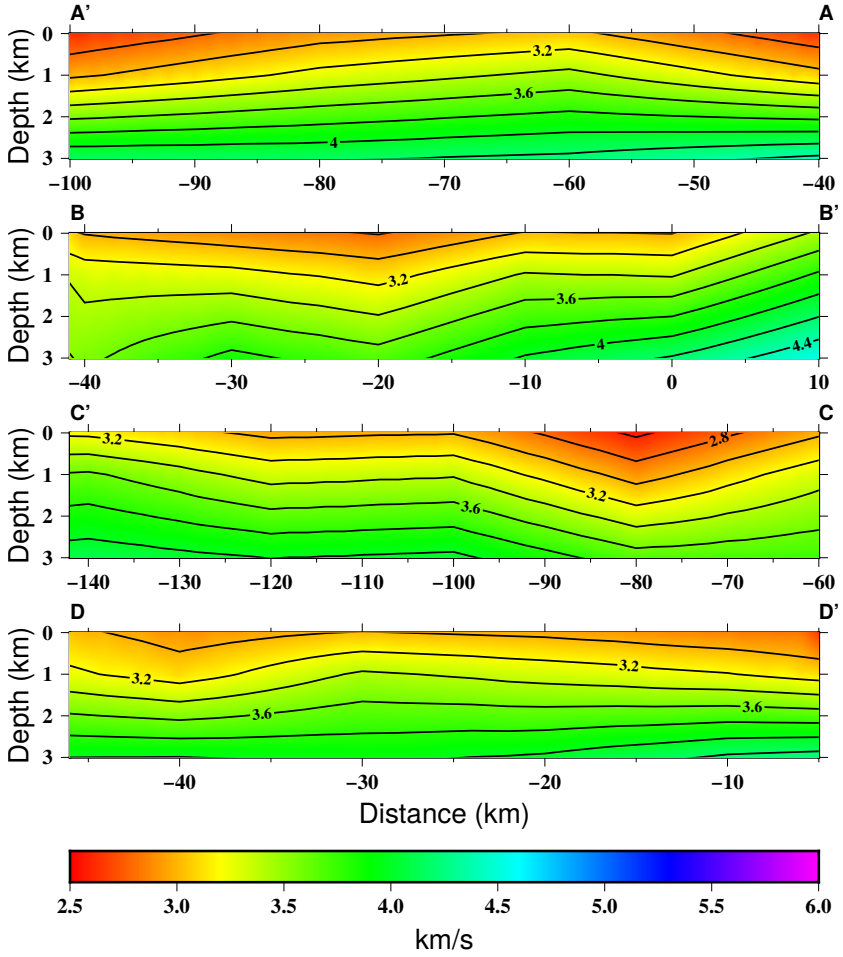

Figure 8: Cross-section slices through SSJD2016 showing the shallow velocity structure. See (Fig. 7) for location of cross sections.

Table 1: Summary of V_p and V_s vs Depth Relations

Relation	**Depth (z) Range***	**Rock Type**
1. $V_p = 0.7 + 42.968z - 575.8z^2 + 2931.6z^3 - 3977.6z^4$	$0 - 0.04$	Quat.-Tertiary sed.
2. $V_p = 1.5 + 3.735z - 3.543z^2$	$0.04 - 0.5$	Quat.-Tertiary sed.
3. $V_p = 2.24 + 0.6z$	$0.5 - 10$	Quat.-Tertiary sed.
4. $V_s = 0.08 + 2.5z$	$0 - 0.025$	Quat.-Tertiary sed.
5. $V_s = (V_p - 1.36)/1.16$	$0.025 - 0.05$	Quat.-Tertiary sed.
6. $V_s = 0.7858 - 1.2344V_p + 0.7949V_p^2 - 0.1238V_p^3 + 0.00064V_p^4$	≥ 0.05	Quat.-Tertiary sed.
7. $V_p = 2.5 + 0.5833z$	$0 - 3.6$	Great Valley sequence
8. $V_s = 0.6 + 1.183z$	$0 - 1$	Great Valley sequence
9. $V_s = 1.5 + 0.2836z$	$1 - 5$	Great Valley sequence
10. $V_p = -0.03 + 2.5 + 2z$	$0 - 1$	Franciscan
11. $V_p = -0.03 + 4.5 + 0.45(z - 1)$	$1 - 3$	Franciscan
12. $V_p = -0.03 + 5.4 + 0.00588(z - 3)$	≥ 3	Franciscan
13. $V_s = 0.7858 - 1.2344V_p + 0.7949V_p^2 - 0.1238V_p^3 + 0.00064V_p^4$	≥ 0	Franciscan
14. $V_p = 1.5 + 5z$	$0 - 0.5$	Granitic rocks
15. $V_p = 4 + 1.3(d - 0.5)$	$0.5 - 1.5$	Granitic rocks
16. $V_p = 5.3 + 0.3(d - 1.5)$	$1.5 - 2.5$	Granitic rocks
17. $V_p = 5.6 + 0.08(z - 2.5)$	$2.5 - 5$	Granitic rocks
18. $V_s = 0.7858 - 1.2344V_p + 0.7949V_p^2 - 0.1238V_p^3 + 0.00064V_p^4$	≥ 0	Granitic rocks
19. $V_p = 5.9$	$0 - 10$	Mafic & GV ophiolite
20. $V_s = 0.7858 - 1.2344V_p + 0.7949V_p^2 - 0.1238V_p^3 + 0.00064V_p^4$	≥ 0	Mafic & GV ophiolite
21. $Q_s = -16 + 104.13V_s - 25.225V_s^2 + 8.2184V_s^3$	≥ 0	All rocks
22. $Q_p = 2Q_s$	≥ 0	All rocks

*V_p in km/s; Depth in km.
From *Aagaard et al.* [2010b]

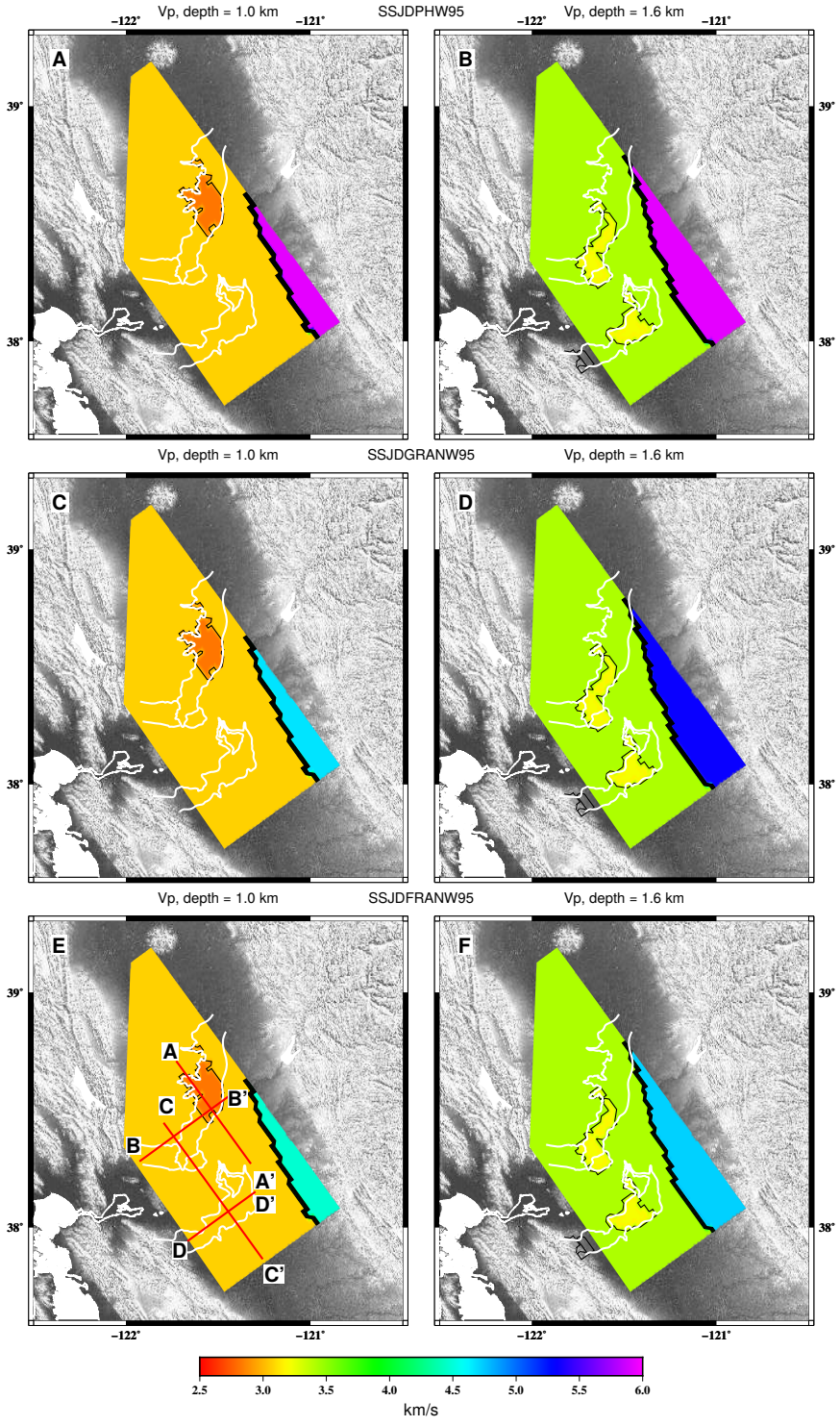

Figure 9: Map-view slices of A and B: SSJDOPHW95 (ophiolite), C and D: SSJDGRAN W95 (granite), and E and F: SSJDFRANW95 (Franciscan) at depths of left: 1.0 km and right: 1.6 km depths. White lines bound the three submarine canyons as projected in the MRF depth-to-sandstone map (*Downey and Clinkenbeard* [2010]). See (Fig. 7) for location of cross sections.

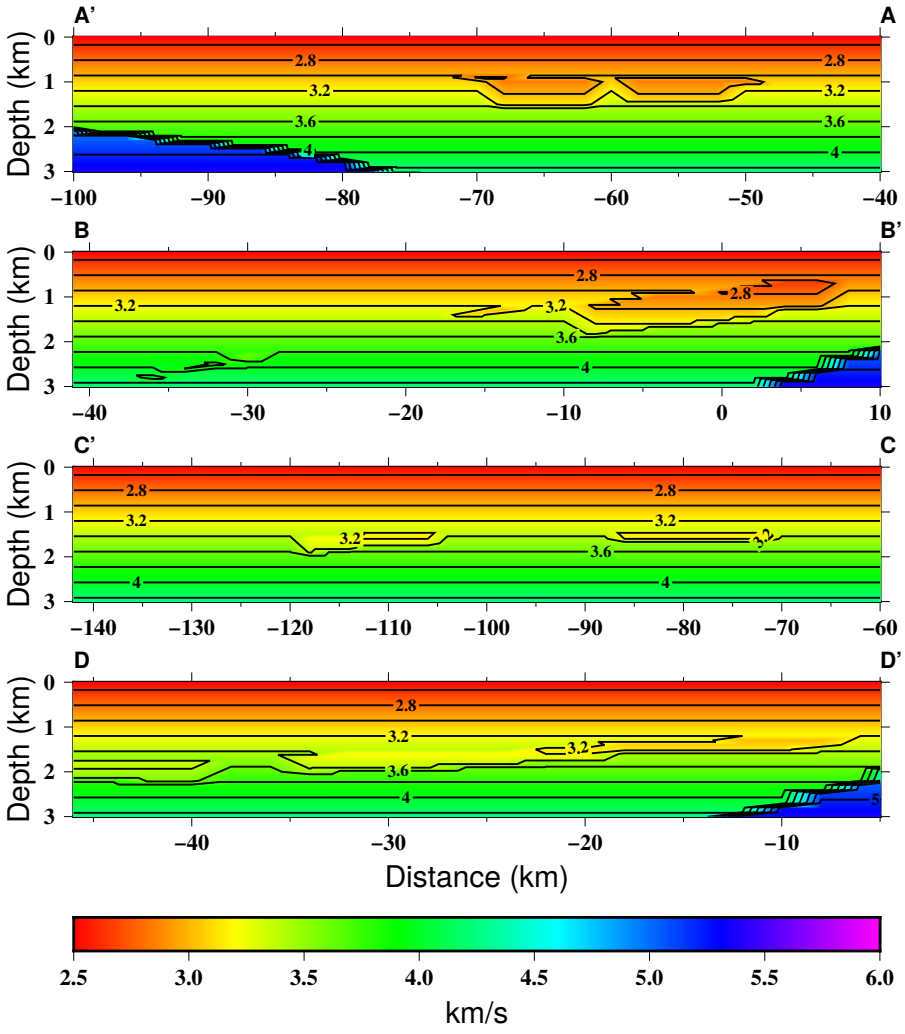

Figure 10: Cross-section slices through SSJDFRANW95 along: (1) A-A', (2) B-B', (3) C-C', and (4) D-D'. Contour interval is 0.2 km/s.

3 Results

The final map-view slices and cross sections for seismic model SSJD2016 are shown in Figure 4. These are cropped to the shallow velocity model area in Figures 7 and 8. Modifications to the shallow subsurface velocities using the Wentworth-basement are shown in Figure 9. Cross sections for SSJDFRANW95 are shown in Figure 10 and are representative of this group of models.

Model data has been archived and is briefly described below. Please see the archived packages for complete data descriptions.

3.1 SSJD2016 Velocity Model Data

filename: vlSSJD2016_2km_xyzltln.txt

format: ascii

parameters: *latitude*, *longitude*, x, y, *depth*, V_p, V_p/V_s, V_s, $DWS - V_p$, and $DRE - V_p$

Comments: Figures of additional depth slices and cross sections are also part of this data package.

doi: 10.5281/zenodo.556605

3.2 Shallow Velocity Model

The shallow velocity model data files contains both the velocity model data and the scripts.

doi: 10.5281/zenodo.569057

format: ascii

Comments: Figures of additional depth slices and cross sections are part of this data package in addition to all report figures.

Script Files

filename: shallownmodelOPH.m

filename: shallownmodelGRAN.m

filename: shallownmodelFRAN.m

Data Files

filename: SSJDshallowmodelOPHW95.out

filename: SSJDshallowmodelGRANW95.out

filename: SSJDshallowmodelFRANW95.out

filename: SJDshallowmodelFRANG16.out

parameters: *longitude*, *latitude*, x, y, *depth*, V_p, V_s, Q_s, and Q_p.

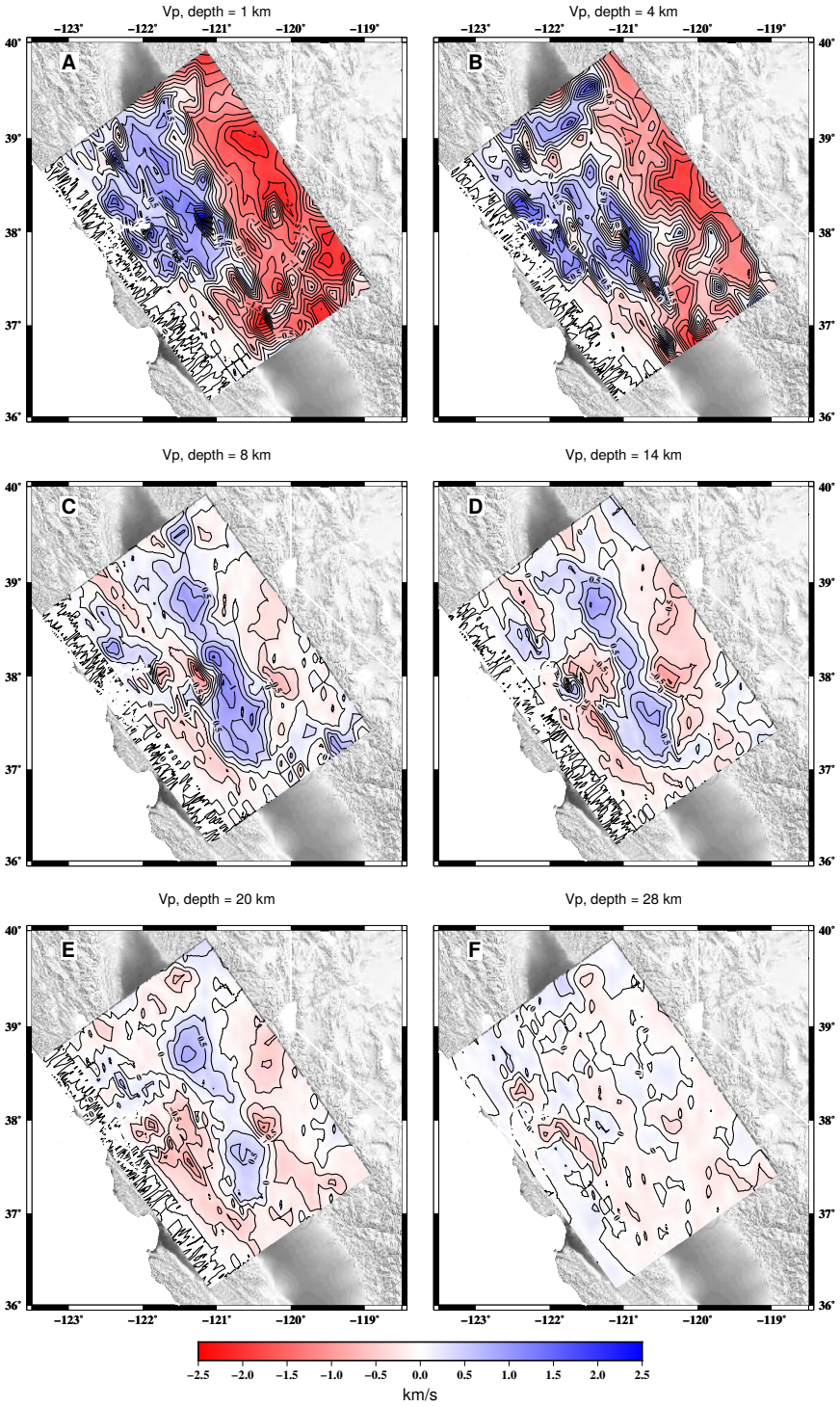

Figure 11: Map-view slices of residuals from SSJD2016 compared to NC2009 at A. 1.0 km, B. 4 km, C. 8 km, D. 14 km, E. 20 km, and F, 28 km depths. Positive residuals represent slower SSJD2016 velocities relative to NC2009 velocities. Negative residuals represent faster SSJD2016 velocities relative to NC2009. Contour interval is 0.25 km/s.

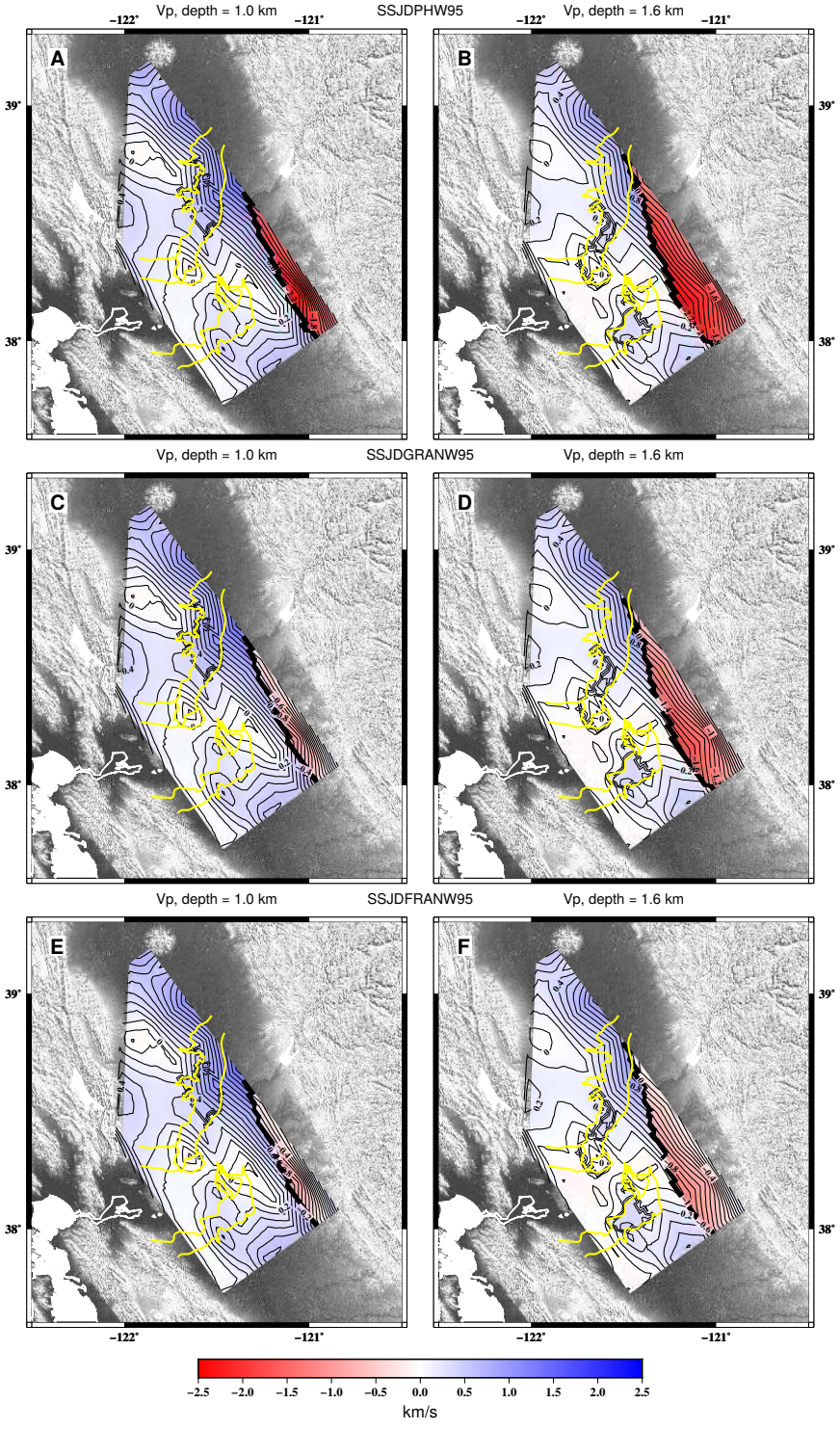

Figure 12: Map-view slices of residuals from SSJDOPHW95 (A and B), SSJDGRANW95 (C and D), and SSJDFRANW95 (E and F) compared to SSJD2016 at 1.0 km (left) and 1.6 km (right) depths. Contour interval is 0.1 km/s. Yellow lines bound the three submarine canyons as projected in the MRF depth-to-sandstone map. Within these models, only the *Wentworth et al.* [1995] basement interpretations are used.

4 Discussion

We improved upon NC2009 in the SSJD by incorporating new travel time data and GV, ambient noise, and gravity measurements. This improved upon the resolution of previous studies especially in regions in which traditional travel time data did not sample in the shallow crust. The differences between NC2009 and SSJD2016 models are predominantly near sea level ($depth = 0$ km). As depth increases, the differences in the model velocities become smaller (Fig. 11). At $depth = 1$ km, SSJD2016 is generally slower than NC2009 west of the Sierra Nevada (SN) and faster ($\sim$1-2.5 km/s) under the SN (Fig. 11A). In the SSJD, SSJD2016 is generally $\sim$1 km/s slower than NC2009. The most noticeable difference exists near Stockton where the SSJD2016 is $\sim$2.6 km/s slower than NC2009. At $depth = 4$ km, SSJD2016 is slower west of the SN and faster under the SN, but the discrepancies are smaller (Fig. 11B). Under the SSJD, the Great Valley south of Stockton, the Coast Ranges west of the SSJD, and just north of Sacramento near the Sutter Buttes, velocities are slower by $0.5 - 1.3$ km/s. Under the SN velocities in SSJD2016 can differ as much as 1.8 km/s. Below 4 km, the velocity differences between the two models decrease to 0.4 km/s (Fig. 11 C-F).

It is well known that an ophiolite sequence underlies the Great Valley group in the Coast Ranges and a magnetic, gravity, and seismic anomaly, possibly another ophiolitic body, exists underneath the Great Valley (*Bailey et al.* [1970]; *Cady* [1975]; *Dickinson et al.* [1996]). The Great Valley Ophiolite (GVO) anomaly extends nearly the entire length of the Sacramento and San Joaquin Valleys (*Cady* [1975]; *Godfrey et al.* [1997]; *Godfrey and Klemperer* [1998]; *Godfrey and Dilek* [2000]; *Moores et al.* [2002]; *Thurber et al.* [2009]; *Lin et al.* [2010]), yet is never exposed in outcrop. Previous models (*Godfrey et al.* [1997]; *Godfrey and Klemperer* [1998]; *Godfrey and Dilek* [2000]) led to interpretations that in northern California the GVO is an unserpentinized mantle section and if present in the southern valley, has been serpentinized to a degree that it cannot be distinguished from Sierran basement. *Moores et al.* [2002] hypothesized that the GVO contains a crustal-mantle sequence that overlies metamorphic belts and a second crustal-mantle sequence. Due to the uncertainty about the composition of the material beneath the Great Valley, we produced the four shallow velocity models each with a different basement rock type and/or basement interpretation. Comparison of the basement map of Graymer (*personal communication*, 2016) and the sandstone isopachs of *Downey and Clinkenbeard* [2010] reveals discrepancies in the western region of the SSJD. In Graymer's map, the basement is only present in the western region where the Coast Range ophiolite is known to be present. SSJDFRANG16 assumes Franciscan basement. The Graymer basement is much shallower than the sandstone depths from *Downey and Clinkenbeard* [2010]. Graymer's basement extends into the sandstone layers defined by *Downey and Clinkenbeard* [2010]. We compared the four velocity models to the new tomography model (SSJD2016). The residuals between SSJD2016 and SSJDOPHW95, SSJDGRANW95, and SSJDFRANW95 are shown in Fig. 12. We favor SSJFRANW95 because it compares well to the tomography (Fig. 12 E and F).

5 Acknowledgements

Waveform data, metadata, and data products for this study were accessed through the Northern California Earthquake Data Center (NCEDC), doi:10.7932/NCEDC. We are grateful to Victoria Langenheim and Russ Graymer for providing gravity data and basement interpretations in the Delta.

6 References

Aagaard, B. T., R. W. Graves, D. P. Schwartz, D. A. Ponce, and R. W. Graymer, Ground-Motion Modeling of Hayward Fault Scenario Earthquakes, Part I: Construction of the Suite of Scenarios, *Bulletin of the Seismological Society of America*, *100*, 2927–2944, 2010a.

Aagaard, B. T., M. G. Knepley, and C. A. Williams, A Domain Decomposition Approach to Implementing Fault Slip in Finite-Element Models of Quasi-static and Dynamic Crustal Deformation, *Journal of Geophysical Research: Solid Earth*, *118*, 3059–3079, 2013.

Aagaard, B. T., R. W. Graves, A. Rodgers, T. M. Brocher, R. W. Simpson, D. Dreger, N. A. Petersson, S. C. Larsen, S. Ma, and R. C. Jachens, Ground-Motion Modeling of Hayward Fault Scenario Earthquakes, Part II: Simulation of Long-Period and Broadband Ground Motions, *Bulletin of the Seismological Society of America*, *100*, 2945–2977, 2010b.

Bailey, E. H., M. Blake Jr, and D. L. Jones, On-land Mesozoic Oceanic Crust in California Coast Ranges, *Geological Survey Professional Paper*, *770-C*, C70–C81, 1970.

Baltay, A. S., and J. Boatwright, Ground-Motion Observations of the 2014 South Napa Earthquake, *Seismological Research Letters*, *86*, 355–360, 2015.

Barnhart, W. D., J. R. Murray, S. Yun, J. L. Svarc, S. V. Samsonov, E. J. Fielding, B. A. Brooks, and P. Milillo, Geodetic Constraints on the 2014 M 6.0 South Napa Earthquake, *Seismological Research Letters*, *86*, 335–343, 2015.

Bennett, J., Vacaville-Winters Earthquakes, 1892, *California Geology*, *40*, 75–83, 1987.

Boatwright, J., J. L. Blair, B. T. Aagaard, and K. Wallis, The Distribution of Red and Yellow Tags in the City of Napa, *Seismological Research Letters*, *86*, 361–368, 2015.

Brocher, T. M., A Regional View of Urban Sedimentary Basins in Northern California Based on Oil Industry Compressional-Wave Velocity and Density Logs, *Bulletin of the Seismological Society of America*, *95*, 2093–2114, 2005a.

Brocher, T. M., Empirical Relations Between Elastic Wavespeeds and Density in the Earth's Crust, *Bulletin of the Seismological Society of America*, *95*, 2081–2092, 2005b.

Brocher, T. M., Compressional and Shear Wave Velocity Versus Depth in the San Francisco Bay Area, California: Rules for USGS Bay Area Velocity Model 05.0.0, *Tech. rep.*, U.S. Geological Survey Open-File Report 05-1317, 2005c.

Brocher, T. M., Compressional and Shear-Wave Velocity versus Depth Relations for Common Rock Types in Northern California, *Bulletin of the Seismological Society of America*, *98*, 950–968, 2008.

Brocher, T. M., et al., The M_w 6.0 24 August 2014 South Napa Earthquake, *Seismological Research Letters*, *86*, 309–326, 2015.

Cady, J. W., Magnetic and Gravity Anomalies in the Great Valley and Western Sierra Nevada Metamorphic Belt, California, *Geological Society of America Special Papers*, *168*, 1–56, 1975.

Dickinson, W. R., et al., Alternate Origins of the Coast Range Ophiolite (California): Introduction and Implications, *GSA Today*, *6*, 1–10, 1996.

Downey, C., and J. Clinkenbeard, Preliminary Geologic Assessment of the Carbon 800 Sequestration Potential of the Upper Cretaceous Mokelumne River, Starkey, and Winters Formations - Southern Sacramento Basin, *PIER Collaborative Report*, *California Energy Commission, Sacramento, CA*, 2010.

Dreger, D. S., M. Huang, A. Rodgers, T. Taira, and K. Wooddell, Kinematic Finite-Source Model for the 24 August 2014 South Napa, California, Earthquake from Joint Inversion of Seismic, GPS, and InSAR Data, *Seismological Research Letters*, *86*, 327–334, 2015.

DRMS, Delta Risk Management Strategy: Probabilistic Seismic Hazard Analysis for Ground Shaking and Estimation of Earthquake Scenario Probabilitiees, *Tech. rep.*, URS Corporation/Jack R. Benjamin & Associates, Inc., 2006.

Eberhart-Phillips, D., and S. Bannister, Three-dimensional Crustal Structure in the Southern Alps Region of New Zealand from Inversion of Local Earthquake and Active Source Data, *Journal of Geophysical Research: Solid Earth*, *107*, ESE 15–1–ESE 15–20, 2002.

Eberhart-Phillips, D., and B. Fry, Joint Surface Wave and Earthquake Travel-Time Inversion for Western North Island, New Zealand, 3-D Velocity Model, *Seismological Research Letters*, *87*, 546, 2016.

Eberhart-Phillips, D., and A. J. Michael, Three-dimensional Velocity Structure, Seismicity, and Fault Structure in the Parkfield Region, Central California, *Journal of Geophysical Research: Solid Earth*, *98*, 15,737–15,758, 1993.

Eberhart-Phillips, D., and M. Reyners, Imaging the Hikurangi Plate Interface Region, with Improved Local-earthquake Tomography, *Geophysical Journal International*, *190*, 1221–1242, 2012.

Field, E. H., T. E. Dawson, K. R. Felzer, A. D. Frankel, V. Gupta, T. H. Jordan, T. Parsons, M. D. Petersen, R. S. Stein, R. J. Weldon, and others, Uniform California Earthquake Rupture Forecast, Version 3 (UCERF3)- The Time-Independent Model, *Bulletin of the Seismological Society of America*, *104*, 1122–1180, 2014.

Fletcher, J. B., and J. Boatwright, Site Response and Basin Waves in the Sacramento-San Joaquin Delta, California, *Bulletin of the Seismological Society of America*, *103*, 196–210, 2013.

Fletcher, J. B., J. Erdem, K. Seats, and J. Lawrence, Tomographic Rayleigh-wave Group Velocities in the Central Valley, California Centered on the Sacramento-San Joaquin Delta, *Journal of Geophysical Research: Solid Earth*, *103*, 2429–2446, 2016, 2015JB012376.

Godfrey, N. J., and Y. Dilek, Mesozoic Assimilation of Oceanic Crust and Island Arc into the North American Continental Margin in California and Nevada: Insights from Geophysical Data, *Ophiolites and Oceanic Crust: New Insights from Field Studies and the Ocean Drilling Program*, *349*, 365–382, 2000.

Godfrey, N. J., and S. L. Klemperer, Ophiolitic Basement to a Forearc Basin and Implications for Continental Growth: The Coast Range/Great Valley Ophiolite, California, *Tectonics*, *17*, 558–570, 1998.

Godfrey, N. J. and Beaudoin, B. C. and Klemperer, S. L. and Mendocino Working Group, Ophiolitic Basement to the Great Valley Forearc Basin, California, from Seismic and Gravity Data: Implications for Crustal Growth at the North American Continental Margin, *Geological Society of America Bulletin*, *109*, 1536–1562, 1997.

Herrmann, R. B., Computer Programs in Seismology: An Evolving Tool for Instruction and Research, *Seismological Research Letters*, *84*, 1081–1088, 2013.

Jachens, R. C., R. W. Simpson, R. W. Graymer, C. M. Wentworth, and T. M. Brocher, Three-Dimensional Geologic Map of Northern California: A Foundation for Earthquake Simulations and Other Predictive Modeling, *Eos Trans. AGU*, *87*, 2006, Fall Meet. Suppl., Abstract S51B-1265.

Langenheim, V. E., R. W. Graymer, and R. C. Jachens, Geophysical Setting of the 2000 M_L 5.2 Yountville, California, Earthquake: Implications for Seismic Hazard in Napa Valley, California, *Bulletin of the Seismological Society of America*, *96*, 1192–1198, 2006.

Lin, G., P. M. Shearer, E. Hauksson, and C. H. Thurber, A Three-dimensional Crustal Seismic Velocity Model for Southern California from a Composite Event Method, *Journal of Geophysical Research: Solid Earth*, *112*, B11,306, 2007, b11306.

Lin, G., C. H. Thurber, H. Zhang, E. Hauksson, P. M. Shearer, F. Waldhauser, T. M. Brocher, and J. Hardebeck, A California Statewide Three-Dimensional Seismic Velocity Model from both Absolute and Differential Times, *Bulletin of the Seismological Society of America*, *100*, 225–240, 2010.

MacKevett, N. H., *Structural Geology of the Sacramento Basin: Pacific Section*, chap. The Kirby Hill Fault Zone, 61–78, Pacific Section of AAPG, 1992.

Moores, E. M., J. Wakabayashi, and J. R. Unruh, Crustal-Scale Cross-Section of the U.S. Cordillera, California and beyond, its Tectonic Significance, and Speculations on the Andean Orogeny, *International Geology Review*, *44*, 479–500, 2002.

NCDEC, Northern California Earthquake Data Center, *UC Berkeley Seismological Laboratory*, *Dataset*, 2014.

Pepper, M. W., and D. S. Johnson, *Structural geology of the Sacramento Basin: Pacific Section*, chap. The Midland Fault System, southern Sacramento basin, California, 27–40, Pacific Section of AAPG, 1992.

Rodgers, A., N. A. Petersson, S. Nilsson, B. Sjgreen, and K. McCandless, Broadband Waveform Modeling of Moderate Earthquakes in the San Francisco Bay Area and Preliminary Assessment of the USGS 3D Seismic Velocity Model, *Bulletin of the Seismological Society of America*, *98*, 969–988, 2008.

Rojstaczer, S. A., R. E. Hamon, S. J. Deverel, and C. A. Massey, Evaluation of Selected Data to Assess the Causes of Subsidence in the Sacramento-San Joaquin Delta, California, *Tech. rep.*, U.S. Geological Survey Open-File Report 91-193, 1991.

Sharma, P., C. E. Jones, J. Dudas, G. W. Bawden, and S. Deverel, Monitoring of Subsidence with UAVSAR on Sherman Island in California's Sacramento-San Joaquin Delta, *Remote Sensing of Environment*, *181*, 218–236, 2016.

Thurber, C., and D. Eberhart-Phillips, Local Earthquake Tomography with Flexible Gridding, *Computers & Geosciences*, *25*, 809–818, 1999.

Thurber, C., H. Zhang, T. Brocher, and V. Langenheim, Regional Three-dimensional Seismic Velocity Model of the Crust and Uppermost Mantle of Northern California, *Journal of Geophysical Research: Solid Earth*, *114*, B01,304, 2009.

Thurber, C. H., T. M. Brocher, H. Zhang, and V. E. Langenheim, Three-dimensional P-wave Velocity Model for the San Francisco Bay Region, California, *Journal of Geophysical Research: Solid Earth*, *112*, B07,313, 2007.

Torres, R. A., N. A. Abrahamson, F. N. Brovold, L. F. Harder, N. D. Marachi, C. H. Neudeck, L. M. O'Leary, M. Ramsbotham, and R. B. Seed, Seismic Vulnerability of the Sacramento-San Joaquin Delta Levees, *Tech. rep.*, Report of Levees and Channels Technical Team, Seismic Vulnerability Sub-team to CALFED Bay-Delta Program, 2000.

Wentworth, C. M., G. R. Fisher, P. Levine, and R. C. Jachens, The Surface of Crystalline Basement, Great Valley and Sierra Nevada, California: A Digital Map Database, *Tech. rep.*, U.S. Geological Survey Open-File Report 95-96, 1995.

Wesling, J. R., and K. L. Hanson, Mapping of the West Napa Fault Zone for Input into the Northern California Quaternary Fault Database, *Tech. rep.*, US Geological Survey External Award Number 05HQAG0002, 2008.

Wong, I. G., *Structural Geology of the Sacramento Basin: Pacific Section*, chap. Earthquake Activity in the Sacramento Valley, California and its Implications to Active Geologic Structures and Contemporary Tectonic Stresses, 5–14, Pacific Section of AAPG, 1992.